

Kondo holes in the 2D itinerant Ising ferromagnet Fe_3GeTe_2

Mengting Zhao^{1,2}, Binbin Chen³, Yilian Xi^{1,2}, Yanyan Zhao⁴, Hongrun Zhang¹, Haifeng Feng^{1,2*}, Jincheng Zhuang¹, Xun Xu^{1,2}, Weichang Hao^{1,3}, Wei Li^{1,3,5*}, Si Zhou^{2,4}, Shi Xue Dou^{1,2}, Yi Du^{1,2*}

¹BUAA-UOW Joint Research Centre and School of Physics, Beihang University, Beijing 100191, China

²Institute for Superconducting and Electronic Materials, Australian Institute for Innovative Materials, University of Wollongong, Wollongong, New South Wales 2500, Australia

³Key Laboratory of Micro-Nano Measurement-Manipulation and Physics (Ministry of Education), Beihang University, Beijing 100191, China

⁴Key Laboratory of Materials Modification by Laser, Ion and Electron Beams, Dalian University of Technology, Dalian 116024, China

⁵International Research Institute of Multidisciplinary Science, Beihang University, Beijing 100191, China

Abstract

Exotic heavy fermion (HF) states emerge in correlated quantum materials with intriguing interplay between localized magnetic moments and itinerant electrons, but they rarely appear in $3d$ -electron systems due to high itinerancy of the d -electrons. The recent discovery of a $3d$ -HF system, Fe_3GeTe_2 (FGT), featuring the coexistence of a Kondo lattice and two-dimensional (2D) itinerant ferromagnetism, provides an exciting platform to explore the origins of d -electron HF states and related emergent phenomena in strongly correlated $3d$ -electron systems. Here, we show that local Fe vacancies in 2D itinerant Ising ferromagnetic FGT are Kondo holes, surrounding which, an anomalous enhancement of Kondo screening has been observed. An itinerant Kondo-Ising model is established, which not only matches the experimental results but also provides insight into the competition between the spontaneous Ising ferromagnetism and the Kondo screening effect in FGT material. The combination of experimental and model analysis explains the microscopic origin of the d -

electron HF states and opens an avenue to study the enriched quantum many-body phenomena with Kondo holes in itinerant Ising ferromagnetic materials.

Introduction

The entanglement and hybridization of local magnetic moments and itinerant electrons lead to the emergence of exotic quantum phases and phenomena, including quantum criticality, topological order, and heavy fermion (HF) metallic behaviour in correlated quantum materials¹⁻⁶. Among others, the HF states in a Kondo lattice model have attracted long-term interest, where the localized moment at each site is screened by the surrounding itinerant electrons and forms a spin singlet. Consequently, significant modulation of the Fermi surface volume and a dramatic increase in the electron effective mass occur when the screening effect appears in the Kondo lattice coherently^{7,8}. Recently, a robust itinerant ferromagnetism with strong out-of-plane anisotropy has been confirmed in a two-dimensional (2D) van der Waals (vdW) Fe₃GeTe₂ (FGT) ferromagnet, even down to monolayers⁹⁻¹⁴. It shows Ising ferromagnetic characteristics with layer-number dependent magnetic phenomena. Remarkably, both HF and Kondo lattice behaviour were observed in this itinerant 2D Ising ferromagnet¹⁵, which is scarce in the 3*d*-electron systems¹⁶⁻¹⁸. This suggests the coexistence of Ising ferromagnetism and electron itineracy in FGT, despite a concrete microscopic modelling of the interplay between the two, is absent, and thus, the origin of the emergent HF states in the 2D Ising ferromagnet remains elusive.

Magnetic vacancies (either non-magnetic substitutions or atomic vacancies) in the Kondo lattice system, known as Kondo holes, are of significance for engineering the HF states by tuning the hybridization between itinerant and localized electrons. Their impacts on the atomic heterogeneity of hybridization and microscopic characteristics of HF states can provide in-depth insight into the complex and competing interactions in Kondo lattice systems¹⁹⁻²¹. In FGT, the Curie temperature, magnetic anisotropy, and net magnetization are

decreased in the presence of Fe vacancies²²⁻²⁵. These vacancies lead to atomic-scale spatial variations in magnetic interactions. In addition, the electronic hybridization of localized and itinerant d -electrons is also expected to be modulated by Fe vacancies. Consequently, the Ising magnetic order and Kondo screening in FGT may vary in the vicinity of Fe vacancies, providing an intricate probe of the Kondo-lattice behaviour and HF states in this 2D Ising ferromagnet.

Here, we reveal the role of intrinsic Fe vacancies as Kondo holes in the 2D magnet, and propose a Kondo-Ising model to understand the origin of HF states in single crystalline FGT. Unusual modulation of hybridization strength due to anomalous enhancement of Kondo screening in the vicinity of each Fe vacancy site has been visualized by measuring the local density of states. Through a comprehensive theoretical analysis using the density functional theory (DFT) and density matrix renormalization group (DMRG) methods, we establish the Kondo-Ising model for HF states in the Ising ferromagnets. We further reveal a concrete scenario for explaining the intriguing interplay between itinerant electrons, local moments, and Kondo holes in the 2D itinerant Ising ferromagnet. The Kondo holes weaken the local magnetic moment by breaking some nearest-neighbouring (NN) “Ising bonds” (i.e., direct spin exchange between $3d$ -electrons) in the ferromagnet, and at the same time, enhance the Kondo screening around it by reducing Pauli exclusion and relieving spin frustration between itinerant electrons. The agreement between experimental observations and the Kondo-Ising model results reveal the intricate role that the Fe vacancy plays in the Ising magnet and confirm FGT as a Kondo-lattice materials with HF states.

Results

The *in-situ* cleaved surface of FGT was first characterized by scanning tunneling microscopy (STM) and scanning tunneling spectroscopy (STS) at 4.2 K. A large-area,

atomically flat surface is shown in **Fig. 1a** (with the inset an optical image of the sample). **Fig. 1b** shows a typical terrace with the height of 8.2 Å, which corresponds to $c/2$ of the FGT lattice. The easily cleaved sample reflects the 2D nature of FGT with a weak vdW interaction between two adjacent Te layers, as illustrated in **Fig. 1d**. In the dI/dV spectrum (**Fig. 1c**), two peaks located at -180 mV and -50 mV can be assigned to the ferromagnetic (FM) states, which are contributed by Fe 3d-states, while the shoulder peak at around 20 mV is attributed to the Kondo resonance (KR) state, which agrees well with a previous study⁸. The STS features give rise to the coexistence of itinerant ferromagnetism and Kondo lattice behaviour in this 3d-electron material. The evolution from the experimental acquired atomic structure by STM, through the simulated STM image to the crystal structure, as calculated by DFT, is shown in **Fig. 1e**, in which good agreement is reached. The brighter and less bright atoms can be assigned to Te and Fe(I) atoms (**Fig. 1e**), respectively, forming a hexagonal lattice with a lattice constant of 4.0 Å.

In the STM image, dark spots can be observed on the FGT surface, as circled in **Fig. 2a**. Although these dark spots are located at Te sites, the height variation between them and the surrounding Te atoms is only 24 pm, which is much smaller than the diameter of a single Te atom (**Fig. S1** in the Supporting Information). Therefore, they are not Te vacancies. Previous studies found that intrinsic Fe vacancies commonly form in FGT single crystal²²⁻²⁵. As Fe(II) sites are right beneath the topmost Te atoms, these dark spots may be reflecting Fe(II) vacancies. We compared dI/dV spectra acquired at the dark spots and surrounding area, as shown in **Fig. 2b** and **2c**. The peaks corresponding to ferromagnetic (FM) states (FM1 and FM2) demonstrate an obvious reduction in intensity, which reflects the lesser contribution to the local density of states (LDOS) from the magnetic Fe atoms. The unoccupied-state LDOS, in contrast, increases when the tip approaches the dark spot, which can be interpreted as a local hole-like doping effect (**Fig. S2**)^{26, 27}. As the Fe vacancies lead to the local deficiency of

electrons, we therefore believe that the dark spots in the STM images are induced by the Fe vacancies at Fe(II) sites. Moreover, the isolated Fe(II) vacancies should not carry magnetic moment, so that they can be regarded as Kondo holes in the FGT Kondo lattice. **Fig. 2c** is a line profile consisting of 30 spectra collected along the dashed line in **Fig. 2d**, which show the spatial distribution of the LDOS of FM as well as Kondo resonance (KR) states. Interestingly, the KR LDOS is enhanced at the Fe(II) vacancy centre and gradually decreases in the vicinity away from the vacancy. This is contrary to intuition in the Kondo lattice model, because a decreased FM LDOS due to Fe(II) vacancies should depress the magnetic moment locally. Consequently, the Kondo screening effect would be reduced and likewise the KR LDOS. The anomalous enhancement in KR LDOS, thus, cannot be explained by the Kondo lattice model for conventional *f*-electron heavy fermion systems.

In order to quantify the impact of the Fe(II) vacancy on the Kondo screening effect, the KR peaks in dI/dV spectra acquired in the Fe(II) vicinity are fitted by using the following Fano resonance line-shape equation²⁸.

$$\frac{dI}{dV} = A_0 + A_K \frac{(q+\varepsilon)^2}{1+\varepsilon^2}, \varepsilon = \frac{eV-\varepsilon_0}{\Gamma} \quad (1)$$

in which, A_0 is a constant, A_K is the Kondo resonance amplitude, q is the Fano symmetry parameter, V is the sample bias voltage, ε_0 is the energy position, and Γ is the resonance half width at the half maximum²⁹. The FM peaks, on the other hand, are also fitted by a Lorentzian line-shape function¹⁵, as shown in **Fig. 3a**. We fitted 11 STS curves taken along the black arrow across an Fe(II) vacancy, as illustrated in the inset of **Fig. 3b**. It is found that the value of q rises from 0.6 at a pristine site to 1.2 at the Fe(II) vacancy site. Together with the enhanced intensity of the KR state (**Fig. 3c**), this implies that enhanced Kondo screening occurred at the Fe(II) vacancy sites. The amplitude of the two FM states decreased as the tip approached closer to the Fe(II) vacancy centre, which is consistent with the large area dI/dV

mapping, as demonstrated in **Fig. S3**. With positive sample bias, electrons tunnel into the unoccupied states of FGT or into the KR which lies close to Fermi level (E_F), as illustrated in **Fig. 3d**. The Fano symmetry parameter q is determined by the ratio of tunnelling probability between the localized KR (t_k) and the direct conducting sea (t_c). A higher probability of tunnelling to the KR state results in higher value of q ³⁰. Unlike the well-studied Kondo impurities of $3d$ metal atom, with a Kondo screening effect that can be decreased by weakened the impurity-substrate interactions²⁹, the Kondo lattice system in FGT with translational symmetry share the same Fermi sea consisted of s/p electrons from Te and Ge atoms, along with delocalized $3d$ electrons and $4s$ electrons of Fe atom. Thus, the enhanced q indicates an enhanced Kondo screening effect, rather than a change in the tunneling probability between the tip and the Fermi sea of the sample.

DFT calculations have been performed to investigate the changes in the electronic structure and itinerant ferromagnetism in the vicinity of Fe(II) vacancies. From a comparison of the electronic structures of pristine (**Fig. 4a**) and defective FGT (**Fig. 4b**), we can see that the Fe(II) vacancy can induce significant hole doping effects and shift the Fermi surface downward (more results in **Fig. S4**), agreeing with our STS measurements and previous angle-resolved photoelectron emission spectroscopy (ARPES) results²⁵. Furthermore, as marked in the **Fig. 4c** and **4d**, there is a notable reduction of spin moment from $2.4 \mu_B$ to $2.1 \mu_B$ for the Fe(I) sites adjacent to the Fe(II) vacancy, accompanied by a higher electron density distribution, which matches well with the weakened FM states in the STS result. Moreover, through DFT calculations of the pristine FGT, we find a prominent FM coupling between nearest neighbour (NN) Fe(I) ions (~ 9 meV) on the same layer. Therefore, direct FM spin exchange between local moments should be included in the theoretical analysis of the Kondo-lattice model for FGT.

To explain the enhancement of the KR in the vicinity of Fe(II) vacancy, we introduce below a Kondo-lattice type many-body microscopic model to fully cover the correlations and hybridization between localized and itinerant electrons in FGT. Considering the two key features of robust ferromagnetism along the c axis, even when FGT is thinned down to a monolayer (due to direct exchange), and strong hybridization between local moments and itinerant electrons, accounting for its large thermal mass and Kondo lattice behaviour^{15,22,23,31,32}, we write down the Kondo-Ising chain Hamiltonian as follows:

$$H = \sum_i J_{Ising} S_i^z S_{i+1}^z + \sum_i J_{Kondo} S_i^a \cdot s_i^b + \sum_i (t_{\parallel} c_i^{\dagger} c_{i+1} + h.c.). \quad (2)$$

The summation (\sum) is over all spin sites other than the hole site located in the middle of the Kondo-Ising chain; S_i^a and s_i^b denote the local moments and spins of the conducting electrons at the i^{th} site, respectively. t_{\parallel} is the hopping amplitude of the conduction electrons between NN sites, J_{Kondo} represents the Kondo coupling between the local moment and the conducting electron at the same local site i , and J_{Ising} represents the ferromagnetic Ising coupling between the NN local moments. The c_i (c_i^{\dagger}) represent the fermion annihilation (creation) operator. The Kondo-Ising chain constitutes a strongly correlated many-body system, and we employed DMRG methods to simulate its ground state. We investigated how the Kondo hole disturbs the hybridization of the localized and itinerant d -electrons, and its effects on the FM order. **Fig. 4e** shows the situation in the pristine FGT Kondo lattice, where the local moments align in a ferromagnetic order and the spin of itinerant electrons partially screen them, showing the Kondo lattice behaviour simultaneously. When a point defect, an Fe vacancy, *i.e.*, a Kondo hole with local moment, is introduced into the system, multiple intriguing consequences emerge, owing to the correlations and hybridization of d -electrons in the system, as shown in **Fig. 4f**. It was found that the expectation value of local moments adjacent to the “hole” are decreased, while the Kondo screening by the spin of itinerant

electrons is enhanced. These simulated results of the Kondo-Ising model well reproduce the experimental observations, and provide insight into the role of Fe vacancy in FGT.

Besides the effects on spin correlations, the Kondo hole has also a strong influence on the charge distribution near the Kondo-hole site (i.e., the centre of the Kondo-Ising chain in the calculations), which can be clearly seen in **Fig. 4g**. By transforming the charge distribution from *real* to momentum (*k*) space, we observe a period-two charge density wave (CDW) pattern that can be recognized by the pronounced peak in the charge structure factor that emerges at π in the vacancy Kondo-Ising system, which is absent in the pristine system (**Fig. 4h**). It is noteworthy that a 2×2 superstructure independent of sample bias and tunnelling distance has been experimentally observed in the dI/dV mapping (**Fig. S5**). Although the one-dimensional (1D) chain model in DMRG calculations is insufficient to imitate the 2D Fermi surface of FGT, the coincidence of the emergence of Fermi surface modification indicates that they very likely share a similar origin. Overall, the DMRG calculations show that the Kondo hole can modify not only the magnetic properties of FGT, including the enhanced Kondo screening of local moments and decreased spontaneous FM ordering, but also alter the Fermi surfaces and charge correlations of itinerant electrons.

Discussion

The relationship between magnetism and Kondo screening in a limited number of *d*-electron systems has been a long-term puzzle, for which a comprehensive understanding of local moments, and itinerant electrons and their interactions is essential. For FGT, the latest ARPES results suggest that local magnetic moments play an indispensable role in the ferromagnetic ordering and electronic structure, which does not fit into the conventional Stoner scenario for itinerant electron ferromagnetism³³. Also, in **Fig. 4a**, our DFT results for the pristine FGT structure show both rather flat and dispersive bands in the *d*-electron

structure, indicating the existence of both localized and itinerant d -electrons in the system. Meanwhile, the local moments in FGT interact with the NN ones in a more direct way – Ising exchange interaction, as confirmed by the DFT calculations, which is very different from the Ruderman–Kittel–Kasuya–Yosida (RKKY) behaviour in f -electron HF systems. On the other hand, our experimental results have clearly revealed a competing interaction between the ferromagnetism and the Kondo effect in FGT, based on their opposite tendency in relation to Kondo holes, which is similar to what occurs in f -electron HF systems despite the very different magnetic interactions.

The reason can be found in the Kondo-Ising model of FGT proposed in this work, as illustrated by the schematic diagrams based on the DMRG calculations (**Fig. 4e** and **4f**). The spins of the itinerant electrons align antiparallel to local moments and induce a Kondo screening of the local moments at each site of the system. On the other hand, the spins of itinerant electrons tend to align antiparallel between NN sites, which is energetically more favourable due to the Pauli exclusion. As the local moments have a strong FM ordering, competition exists between FM and Kondo screening that actually leads to spin frustration. This spin frustration is locally relieved by the presence of a Kondo hole. As shown in **Fig. 4f**, the spins of itinerant electrons in the close vicinity of the Kondo hole can preferentially align parallel to the local moments forming the Ising FM order, which, in turn, enhances the Kondo screening effect on the adjacent local moments. Similar competition between the $3d$ -electron FM and the Kondo effect has been observed by STS in cobalt dimers³⁴ and quantum point contacts of Fe/Co/Ni transition metal, indicating that the way of exchange coupling of the $3d$ -electron magnetic moments is critical for forming the Kondo screening³⁵. More importantly, due to the Ising interaction in FGT, stronger local Kondo screening due to the presence of Kondo holes can enhance the hybridization between the adjacent local moments and itinerant electrons, rather than simply destroying the coherence of the Kondo lattice as in f -electron

systems, as exemplified in Th doped URu₂Si₂^{20, 21}. In addition to the Kondo screening itself, many studies have shown that the electron effective mass in FGT is very sensitive to a deficiency of Fe atoms, despite the absence of notable internal tensile stress existing in Kondo-hole substitution. The enhanced local Kondo screening induced by Kondo holes, as revealed in the present study, thus, may explain the change in the electron effective mass through enhancing the hybridization between local moments and spins of itinerant electrons.

Conclusion

In summary, we have performed STM and STS measurements on FGT, with an emphasis on the effects of Fe vacancy, i.e., Kondo holes. Decreased ferromagnetism and enhanced Kondo screening in the vicinity of a Kondo hole were revealed and explained. By combining the experimental results with DFT and DRMG calculations, a concrete Kondo-Ising scenario for the strongly correlated *d*-electrons in FGT has been established, which can not only describe the competing relationship between the Kondo screening effect and Ising ferromagnetism, but also reveals the origin of the HF behaviour in FGT. This clarification of the role of Fe vacancies as Kondo holes in ferromagnetic and HF behaviour in FGT can enrich our understanding of the ferromagnetism and electronic properties of the 2D Ising ferromagnet FGT, and paves the way to their spintronic engineering and application.

Notes: The authors declare no competing financial interest.

Acknowledgements

This work was supported by the Australian Research Council (DP170101467, FT180100585 and LP180100722) National Key R&D Program of China (2018YFE0202700), and National Natural Science Foundation of China (Nos. 11874003, 11974036, 11834014, 11904015, 51672018) and Beijing Natural Science Foundation (Z180007). The work was partially supported by the

UOW-BUAA Joint Research Centre and a Vice Chancellor's Research Fellowship from the University of Wollongong. The authors acknowledge the computer resources provided by the NCI National Facility through the University of Wollongong Partner Share Scheme, and the Supercomputing Centre of Dalian University of Technology. We thank Professor Lan Wang, Professor Jiabao Yi, Professor Lan Chen, and Professor Faxian Xiu for valuable discussions and communications, and Dr Tania Silver for critical reading of the manuscript.

References

- [1] Mathur, N. D. et al. Magnetically mediated superconductivity in heavy fermion compounds. *Nature* **394**, 39-43 (1998).
- [2] Si, Q., Rabello, S., Ingersent, K., & Smith, J. L. Locally critical quantum phase transitions in strongly correlated metals. *Nature* **413**, 804-808 (2001).
- [3] Coleman, P., & Schofield, A.J. Quantum criticality, *Nature* **433**, 226-229 (2005).
- [4] Stewart, G. R. Non-Fermi-liquid behaviour in *d*- and *f*-electron metals. *Rev. Mod. Phys.* **73**, 797–855 (2001).
- [5] Chubukov, A. V., Pépin, C. & Rech, J. Instability of the quantum critical point of itinerant ferromagnets. *Phys. Rev. Lett.* **92**, 147003 (2004).
- [6] Shen, B. et al. Strange-metal behaviour in a pure ferromagnetic Kondo lattice. *Nature* **579**, 51-55 (2020).
- [7] Coleman, P. Heavy Fermions and the Kondo Lattice: A 21st Century perspective. *Forschungszentrum Jülich*, **5**, 21 (2015).
- [8] Si, Q., Steglich, F. Heavy fermions and quantum phase transitions. *Science* **329** 1161-1166 (2010).

- [9] Fei, Z. et al. Two-dimensional itinerant ferromagnetism in atomically thin Fe_3GeTe_2 . *Nature Mater.* **17**, 778–782 (2018).
- [10] Deng, Y. et al. Gate-tunable room-temperature ferromagnetism in two-dimensional Fe_3GeTe_2 . *Nature* **563**, 94–99 (2018).
- [11] Xiao, W. et al. Current-driven magnetization switching in a van der Waals ferromagnet Fe_3GeTe_2 . *Sci. Adv.* **5**, eaaw8904 (2019).
- [12] Shanshan, L. et al. Wafer-scale two-dimensional ferromagnetic Fe_3GeTe_2 thin films grown by molecular beam epitaxy. *npj 2D Mater. Appl.* **1**, 30 (2017).
- [13] Tan, C. et al. Hard magnetic properties in nanoflake van der Waals Fe_3GeTe_2 . *Nat Commun.* **9**, 1554 (2018).
- [14] Mohammed, A. et al. Highly Efficient Spin–Orbit Torque and Switching of Layered Ferromagnet Fe_3GeTe_2 . *Nano Lett.* **19**, 4400–4405 (2019).
- [15] Zhang, Y. et al. Emergence of Kondo lattice behaviour in a van der Waals itinerant ferromagnet Fe_3GeTe_2 . *Sci. Adv.* **4**: eaao6791 (2018).
- [16] Urano, C. et al. LiV_2O_4 Spinel as a Heavy-Mass Fermi Liquid: Anomalous Transport and Role of Geometrical Frustration. *Phys. Rev. Lett.* **85**, 1052 (2000).
- [17] Wu, Y. P. et al. Emergent Kondo Lattice Behavior in Iron-Based Superconductors AFe_2As_2 ($\text{A}=\text{K}, \text{Rb}, \text{Cs}$). *Phys. Rev. Lett.* **116**, 147001(2016).
- [18] Hisashi, K. et al. Helimagnetic Structure and Heavy-Fermion-Like Behavior in the Vicinity of the Quantum Critical Point in Mn_3P . *Phys. Rev. Lett.* **124**, 087202(2020).
- [19] Thompson, J. D. Holes in a Kondo lattice. *Proc. Natl. Acad. Sci.* **108**, 18191 (2011)

- [20] Hamidian, M. H. et al. How Kondo-holes create intense nanoscale heavy-fermion hybridization disorder. *Proc. Natl. Acad. Sci.* **108**, 18233 (2011)
- [21] Schmidt, A. et al. Imaging the Fano lattice to ‘hidden order’ transition in URu₂Si₂. *Nature* **465**, 570–576 (2010).
- [22] Verchenko, V. Y. Ferromagnetic order, strong magnetocrystalline anisotropy, and magnetocaloric effect in the layered Telluride Fe_{3-δ}GeTe₂ *Inorg. Chem.* **54**, 17, 8598-8607 (2015).
- [23] May, A. F., Calder, S., Cantoni, C., Cao, H., & McGuire, M. A., Magnetic structure and phase stability of the van der Waals bonded ferromagnet Fe_{3-x}GeTe₂ *Phys. Rev. B* **93**, 014411 (2016).
- [24] Kim, K. et al. Large anomalous Hall current induced by topological nodal lines in a ferromagnetic van der Waals semimetal. *Nat. Mater.* **17**, 794–799 (2018).
- [25] Park, S. Y. et al. Controlling the magnetic anisotropy of the van der Waals ferromagnet Fe₃GeTe₂ through Hole Doping. *Nano Lett.* **20**, 95-100 (2020).
- [26] Wong, D. et al. Characterization and manipulation of individual defects in insulating hexagonal boron nitride using scanning tunnelling microscopy. *Nat. Nanotech.* **10**, 949–953 (2015).
- [27] Wang, Y. et al. Mapping Dirac quasiparticles near a single Coulomb impurity on graphene. *Nat. Phys.* **8**, 653–657 (2012).
- [28] Moro-Lagares, M. et al. Real space manifestations of coherent screening in atomic scale Kondo lattices. *Nat. Commun.* **10**, 2211 (2019).
- [29] Otte, A. F. et al. The role of magnetic anisotropy in the Kondo effect. *Nat. Phys.* **4**, 847–850 (2008).

- [30] Ternes, M., Heinrich, A. J, & Schneider, W-D. Spectroscopic manifestations of the Kondo effect on single adatoms. *J. Phys.: Condens. Matter* **21**, 053001 (2009).
- [31] Chen, B. Magnetic properties of layered itinerant electron ferromagnet Fe₃GeTe₂. *J. Phys. Soc. Jpn.* **82**, 124711 (2013).
- [32] Zhu, J.-X. et al. Electronic correlation and magnetism in the ferromagnetic metal Fe₃GeTe₂. *Phys. Rev. B* **93**, 144404 (2016).
- [33] Xu, X. et al. Signature for non-Stoner ferromagnetism in the van der Waals ferromagnet Fe₃GeTe₂. *Phys. Rev. B* **101**, 201104 (2020).
- [34] Chen, W., Jamneala, T., Madhavan, V., & Crommie, M. F. Disappearance of the Kondo resonance for atomically fabricated cobalt dimers. *Phys. Rev. B*, **60**, R8529 (1999).
- [35] Calvo, M. et al. The Kondo effect in ferromagnetic atomic contacts. *Nature* **458**, 1150–1153 (2009).

Figures and Figures Captions

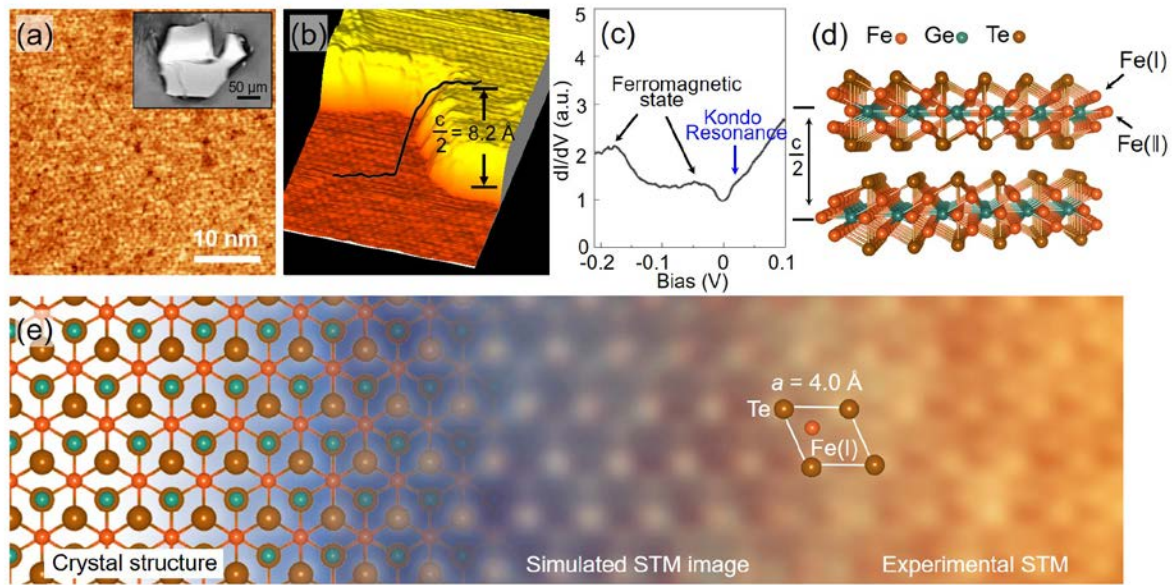


Fig. 1: Crystal and electronic structure of FGT. (a) Large-scale STM image of the surface of FGT (001) single-crystal. Inset: Optical image of FGT single-crystal. (b) Atom-resolved STM topography at 4.2 K with 9 mV of sample bias. (c) dI/dV curves for FGT at 4.2 K ($I_{setpoint} = 300 \text{ pA}$). (d) Side views of the crystal structure of FGT. (e) Schematic diagram of the evolution from the atomic structure of FGT along the [001] direction to the simulated STM image and then to the experimental STM image (40 mV, 2.8 nA) (from left to right).

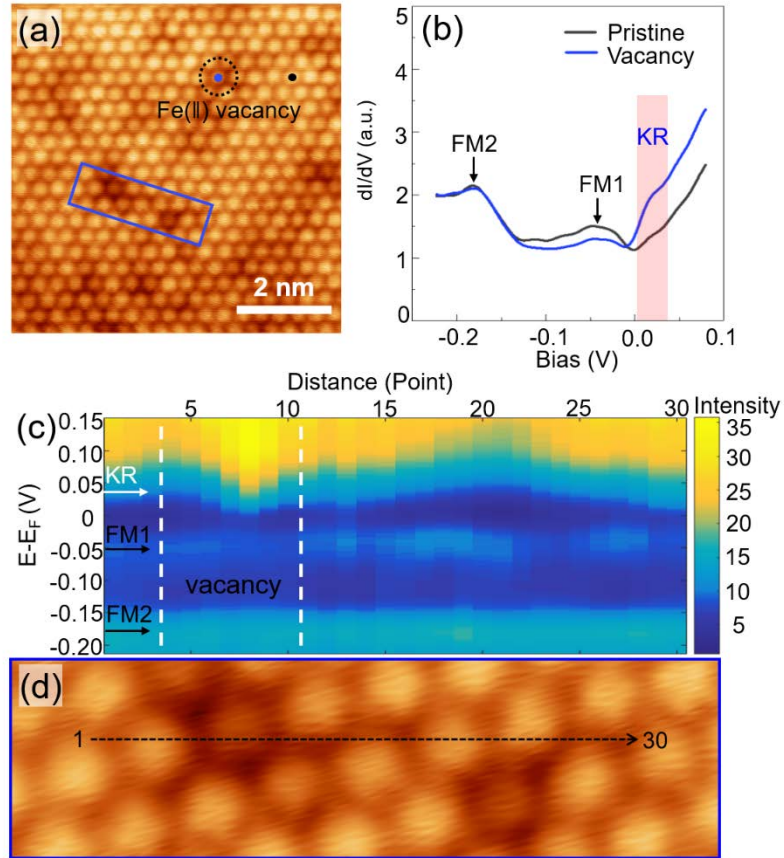


Fig. 2: Fe(II) vacancy characteristics in the FGT. (a) Atomic-resolution STM image (-200 mV, 400 pA) of FGT with Fe(II) vacancies. The black dotted circle identifies the Fe(II) impurity. (b) A pair of dI/dV spectra taken over areas with a vacancy (blue dot in a) and far away from a vacancy (black dot in a). (c) Waterfall image of 30 successive dI/dV curves measured along the broken line in (d). (d) Zoomed STM image of the area marked by the blue rectangle in (a).

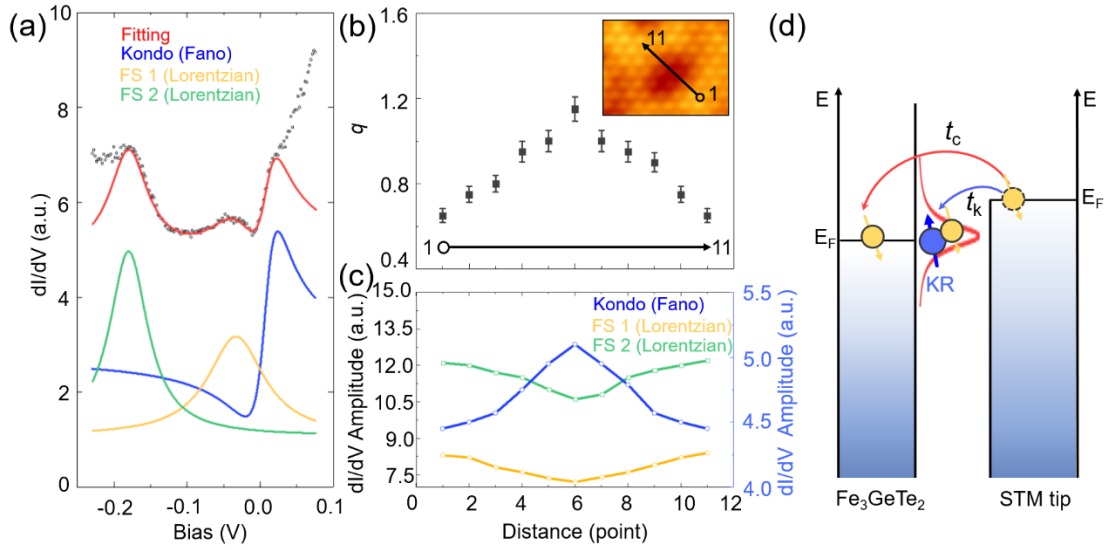


Fig. 3: Analysis of the STS curves of FGT. (a) Theoretical fitting of experimental dI/dV curves. The blue curve is a Fano fit with the best fit parameters of $q = 1.40 \pm 0.04$, $\Gamma = 34 \pm 5$ mV. After analysis of 11 successive experimental dI/dV curves using the method shown in (a), (b), and (c), it is found that the q and the amplitude depend on the distance from the vacancy, respectively. The inset shows these 11 points are obtained along the line crossing a vacancy. (d) Schematic illustration of the tunnelling process in the STS measurement of FGT: the electrons (yellow circle with arrow) will tunnel from the STM tip into the continuum of FGT or the Kondo resonance state right at the Fermi sea of FGT. The probability of these tunnelling processes are labelled as t_c and t_k , respectively. The blue circle with an arrow represents the local moment of an Fe atom.

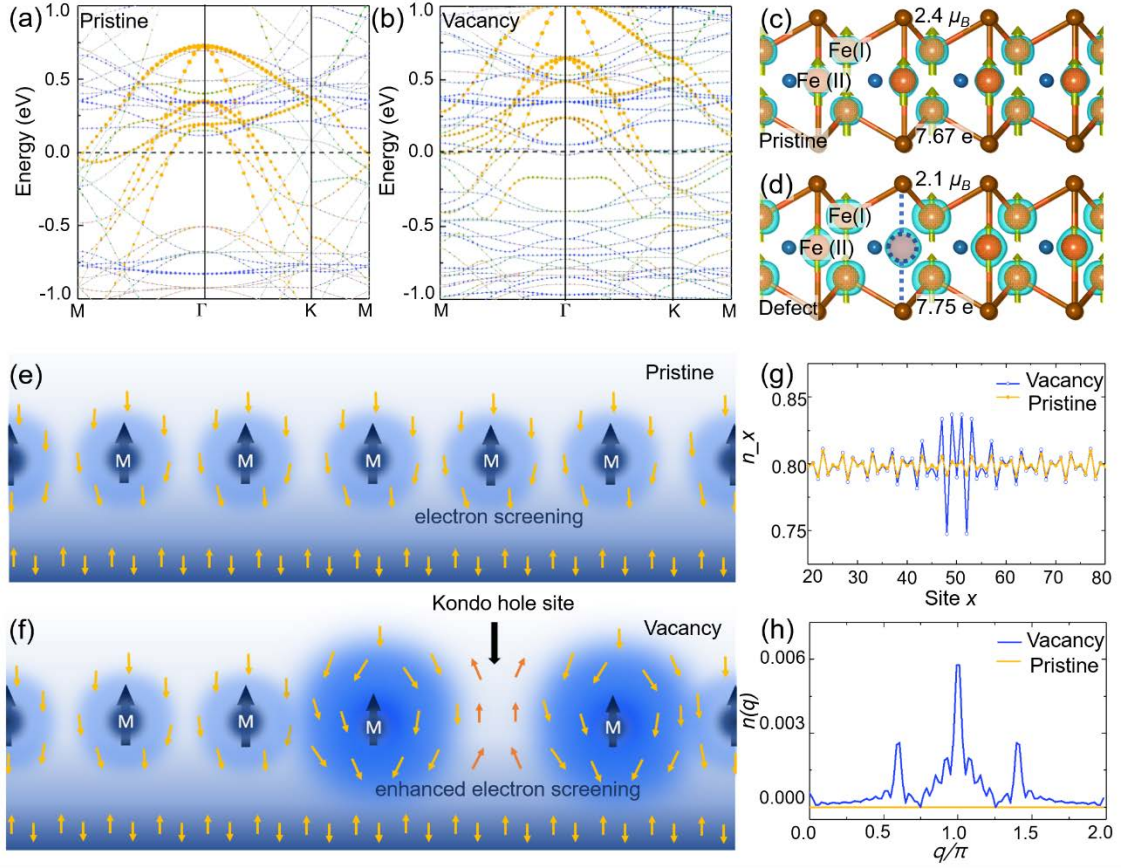


Fig. 4: Theoretical simulation of the effects of Fe(II) vacancies on the FGT. (a) and (b) are electronic structures for pristine Fe_3GeTe_2 and Fe_3GeTe_2 with vacancies, respectively. (c) and (d) are the side views of the crystal structures for these two situations. The blue atmosphere around the Fe atom represents the charge distribution. (e) and (f) are schematic diagrams of the Kondo screening in a pristine Kondo lattice and in a lattice with a Kondo hole, respectively. (g) and (h) are the real space charge density distribution and the corresponding momentum-space structures, respectively. $n(q) = \sum_{x=1}^L e^{jqx} (n_x - n_0)$ is the Fourier transform of the real-space distribution n_x at site x (with the background of average electron occupation, $n_0 = \bar{n}_x$ subtracted).